

Self-Adaptive Monolithic Anthropomorphic Finger with Teeth-Guided Compliant Cross-Four-Bar Joints for Underactuated Hands

Guochao Bai and Nicolas Rojas, *Member, IEEE*

Abstract—This paper presents a novel approach for modeling one-degree-of-freedom human metacarpophalangeal/ interphalangeal joints based on a teeth-guided compliant cross-four-bar linkage. The proposed model allows developing self-adaptive anthropomorphic fingers able to be 3D printed in a single step without any accessories, except for simple tendon wiring after the printing process, using basic single-material additive manufacturing. Teeth-guided compliant cross-four-bar linkages as finger joints not only provide monolithic fabrication without assembly but also increase precision of anthropomorphic robot fingers by removing nonlinear characteristics, thus reducing the complexity of control for delicate grasping. Kinematic analysis of the proposed compliant finger joints is detailed and nonlinear finite element analysis results demonstrating their advantages are reported. A two-fingered underactuated hand with teeth-guided compliant cross-four-bar joints is also developed and qualitative discussion on grasping is conducted.

I. INTRODUCTION

The study on human hand shows that anatomical structure and nervous system have significant contribution for hand ability [1]. Joints of human hand have complex non-symmetric surfaces and produce more complex movements than the revolute motion usually associated to them [2]. Design of versatile and robust robotic hands of low complexity that have same functions as the human hand is still a challenging work despite the progress made in the last decades [3], [4], [5], [6]. However, the evolution and anatomy research on human hand still provide new perspectives to design robotic hands [7], [8], [9], [10]. Conversely, it can be argued that the design of anthropomorphic robotic hands can help obtaining a better understanding of how human hands operate and are controlled.

Simple revolute joints are commonly utilized in robotic hands because of their simplicity and functionality. However, this approach fails to reproduce properly the operation of human finger joints which conduct polycentric motion during flexion and extension. That means the intersection point of axes of adjacent finger segments is always changed during motion. Research has been indeed carried out on replicating human joints without the use of revolute pairs. For instance, a metacarpophalangeal (MCP) joint with biomechanics and dynamic properties close to human counterparts based on a combination of a ball joint, crocheted ligaments, and a silicon rubber sleeve was developed in [11]. A joint type based on contact-aided design of phalanxes was introduced in

This work was supported in part by the Engineering and Physical Sciences Research Council grant EP/R020833/1.

Guochao Bai and Nicolas Rojas are with the REDS Lab, Dyson School of Design Engineering, Imperial College London, 25 Exhibition Road, London SW7 2DB, UK. E-mail: {g.bai, n.rojas}@imperial.ac.uk.

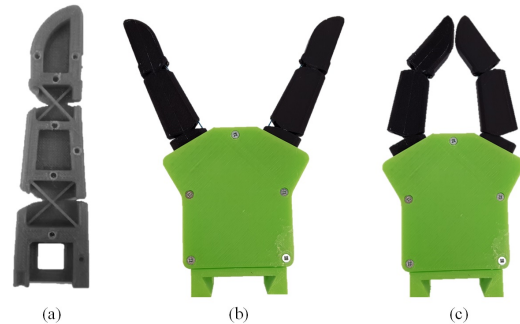


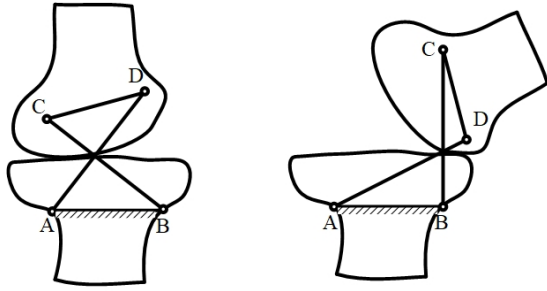
Fig. 1. A two-fingered underactuated robotic hand composed of anthropomorphic fingers with teeth-guided compliant cross-four-bar joints. These fingers can be fabricated in a single step using basic single-material 3D printers, just requiring simple tendon wiring after the printing process. Section clipped finger (a); front view, hand open (b); and front view, hand closed (c).

[12]. A novel design of a compliant rolling-contact element capable of performing the functions of a bearing and a spring is presented in [13]. A rotational sliding joint was developed and some other issues on underactuated tendon-driven robotic hands also addressed in [14]. In [15], an anthropomorphic finger with contact-aided surface and rigid cross-four-bar joints was investigated; the use of these rigid linkages results in high friction and a complicate assembly process.

Since linkages in biological systems are usually compliant and always formed by ligaments [16], compliant mechanisms and structures have also been applied for development of robotic grippers and hands. Some single-piece flexible grippers have been also developed with distributed compliance structure [17], [18], [19] or flexible joints [20], [21], [22], [23]. However, anthropomorphic design of monolithic robotic fingers has not been explored so far.

In this paper, a novel type of anthropomorphic finger based on teeth-guided compliant linkage joints is presented Fig. 1(a). The introduced fingers can be fabricated in a single step using basic single-material 3D printers, just requiring simple tendon wiring after the printing process. The monolithic finger comprises compliant cross-four-bar joints with teeth-guided contact surface that makes the joint motion both easy and precise to control. A two-fingered underactuated hand composed of the proposed fingers is also developed Fig. 1(a) and (b), with a qualitative discussion on its grasping capabilities.

The rest of this paper is organised as follows. In section II four-bar linkages for biological morphology are introduced.



(a) Initial position of knee linkage (b) Final position of knee linkage

Fig. 2. Cross-four-bar mechanism in human knee joint

section III investigates the kinematics of cross-four-bar linkages. The mathematical method to generate moving and fixed centrodes is presented. Anthropomorphic joints based on compliant cross-four-bar linkages with contact-aided and teeth-guided surfaces are analyzed in section IV. A two-fingered anthropomorphic hand with differential transmission mechanism using the proposed fingers is then prototyped and tested in section V. Finally, we conclude in section VI.

II. FOUR-BAR LINKAGE FOR BIOLOGICAL MORPHOLOGY

Research shows that linkages are widely distributed in animals skeleton systems. A classification system has been designed to suit for biological systems [24]. A well-known substitution of human knee joint is cross-four-bar linkages. As shown in [25], cross-four-bar linkage was utilized to replicate the polycentric motion of the knee that occurs during passive knee flexion-extension. A cross-four-bar mechanism was also proposed in [26] for the knee design of bipedal robot. As depicted in a lateral view in Fig. 2, the anterior and posterior cruciate ligaments connecting the upper femur and the lower tibia cross each other. AB and CD represent the femur and tibia while BC and AD represent two ligaments. The ideal configuration allows the femur to roll on the tibia without friction. The contact-aided cross-four-bar mechanism is a better option to design artificial knee joint prosthetics than pin joint. An artificial foldable hinged wing based on two cross-four-bar linkages was developed to mimic the behaviours of the beetles hind wing [27]. Applications on robotic hands for motion imitation also existed in [15] and [28].

Concave four-bar linkages as another biological linkages are also widely distributed in animals. Fig. 3(a) shows a mantis shrimps strike which generates extremely rapid speed and high force [29]. Morphological analysis shows that a concave four-bar linkage is the main kinematic component which amplifies rotation in the system. Fig. 3(b) is another concave isosceles four-bar linkage in teleost fish [30]. Force-amplification occurs when the hyoid bars are close to the in-line position. In this mechanism, a weak input can produce a very large output force.

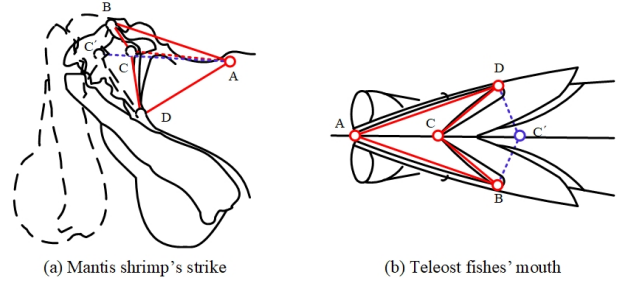


Fig. 3. Concave four-bar linkages in biological systems

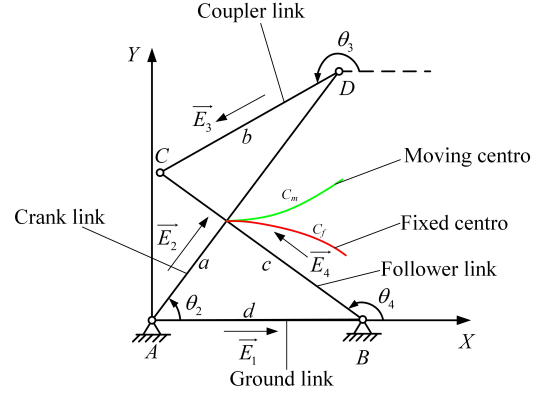


Fig. 4. Position vector loop of cross-four-bar linkage and centrodes

III. KINEMATICS OF CROSS-FOUR-BAR MECHANISM

Cross-four-bar linkage and its biological morphology were addressed in section II. In this section, the kinematics of a cross-four-bar mechanism will be investigated. The centrodes of this mechanism are to be explored. Contact-aided cross-four-bar mechanism is addressed to mimic the complex movements of finger joints. The contact surface increases stiffness of cross-four-bar linkage. The centrode, an important characteristic in planar kinematics, is a path traced by the instantaneous centre of rotation of a rigid link moving in a plane [31]. The motion of the coupler link with respect to the ground link is pure rotation around the instantaneous centre. The fixed centrode can be found by tracing the intersection of the crank link and follower link. For crossing linkages, the length of one diagonal increases if, and only if, the other decreases [32].

Figure 4 shows the cross-four-bar linkage and its fixed and moving centrodes. Four links of the cross-four-bar mechanism AD , CD , BC , AB are indicated by a , b , c and d respectively. C_m and C_f respect moving and fixed centrodes, respectively. θ_2 , θ_3 and θ_4 are four orientation angles of link vectors. The links are now drawn as position vectors that form a vector loop with the vector loop equation is

$$\vec{E}_2 + \vec{E}_3 - \vec{E}_4 - \vec{E}_1 = 0. \quad (1)$$

The solution of Equation (1) can be expressed as [33]

$$\theta_{4,2} = 2 \arctan\left(\frac{-N \pm \sqrt{N^2 - 4MP}}{2M}\right) \text{ and} \quad (2)$$

$$\theta_{3,2} = 2 \arctan\left(\frac{-N \pm \sqrt{N^2 - 4QR}}{2Q}\right) \quad (3)$$

where

$$M = \cos \theta_2 - K_1 - K_2 \cos \theta_2 + K_3,$$

$$N = -2 \sin \theta_2,$$

$$P = K_1 - (K_2 + 1) \cos \theta_2 + K_3,$$

$$Q = \cos \theta_2 - K_1 + K_4 \cos \theta_2 + K_5,$$

$$R = K_1 - (K_4 - 1) \cos \theta_2 + K_5,$$

$$K_1 = \frac{d}{a},$$

$$K_2 = \frac{d}{c},$$

$$K_3 = \frac{a^2 - b^2 + c^2 + d^2}{2ac},$$

$$K_4 = \frac{d}{b}, \text{ and}$$

$$K_5 = \frac{c^2 - d^2 - a^2 - b^2}{2ab}.$$

Equations (2) and (3) have two solutions. According to Grashof condition, if the sum of the shortest and longest links of a planar quadrilateral linkage is less than or equal to the sum of the remaining two links, then the shortest link can rotate fully with respect to a neighbour link. That means, only those cross-four-bar mechanisms satisfied with the condition $s + l \leq p + q$ are considered where s is the shortest link, l is the longest, and p and q are the other links. A Grashof linkage is defined as crossed if the two links adjacent to the shortest link cross one another and open if they don't cross one another in this position [33]. The discrimination under the radical is positive and the solution is not complex conjugate. There are two values of θ_3 and θ_4 corresponding to any one value θ_2 . These are referred to the crossed and open linkage configurations or the linkage two circuits (Fig. 5) [34]. In addition, the two shortest links ($AB = CD$) are also contained in the Grashof linkage. In other words, the cross-four-bar mechanisms can be obtained by using the Grashof condition and the shortest rule.

According to Kennedy-Aronhold theorem [35], the centre is found at the intersection of the extensions of the crank and the follower. In the case of cross-four-bar mechanism, the centre is always between the coupler link and the ground link. As shown in Fig. 6, AB is fixed as a frame and AD rotates clockwise with respect to A . The locus of centres of instantaneous rotation for D is a line along AD and for C is the line along CB . Therefore, the instantaneous centre of rotation for coupler link CD is C_f , the crossing point of AD and CB . Assuming A is the original position of the fixed coordinate frame, the fixed centre is the crossing point of two vector \vec{AD} and \vec{BC} . Therefore, the locus of

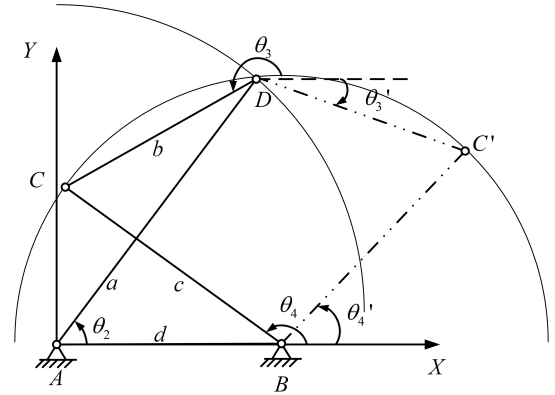


Fig. 5. Two solutions to the crossed and open configurations of the four-bar linkage

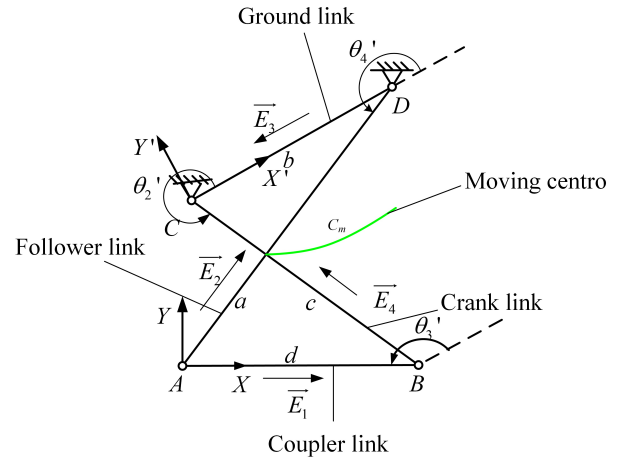


Fig. 6. Moving centres at coordinate frame $X'CY'$

fixed centres can be expressed as

$$\vec{C}_f = \frac{a \tan \theta_4}{\tan \theta_2} + j \frac{a \tan \theta_4 \tan \theta_2}{\tan \theta_4 - \tan \theta_2}, \quad (4)$$

where θ_2 is an independent variable and θ_4 can be obtained from Equation (2).

The moving centres can be obtained by attaching the coordinate frame to coupler link CD with C as the original point and having the same rotation with angle DCB decreasing, as shown in Fig. 6. By using the same expression method, the vector of the moving centres with respect to the coordinate frame $C - X'Y'$ can be expressed as

$$\vec{C}_m = \frac{b \tan \theta'_4}{\tan \theta'_4 + \tan \theta'_2} + j \frac{b \tan \theta'_4 \tan \theta'_2}{\tan \theta'_4 - \tan \theta'_2}, \quad (5)$$

where

$$\theta'_4 = -3\theta_2 - \theta_3 \text{ and} \quad (6)$$

$$\theta'_2 = \theta_4 - 2\theta_2 - \theta_3. \quad (7)$$

The transformation matrix of coordinate frame $C - X'Y'$

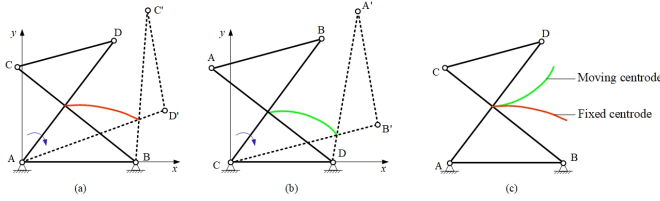


Fig. 7. Centroides of cross-four-bar mechanism

with respect to frame $A - XY$ is expressed as

$${}^C_A T = \begin{bmatrix} -\cos(2\theta_2 + \theta_3) & \sin(2\theta_2 + \theta_3) & a \cos \theta_2 + b \cos \theta_3 \\ -\sin(2\theta_2 + \theta_3) & -\cos(2\theta_2 + \theta_3) & a \sin \theta_2 + b \sin \theta_3 \\ 0 & 0 & 1 \end{bmatrix}. \quad (8)$$

The vector of moving centrode with respect to the coordinate system XAY can be expressed as

$$\vec{C}_m = {}^C_A T \vec{C}'_m. \quad (9)$$

Partial trajectories of centroides with a rotational angle of the crank link of 80 degrees are shown in Fig. 7. The motion of the coupler link with respect to the ground link is duplicated by making these two centroides roll against one another without slipping. Due to the pure rolling of the two curves, they have the same length.

IV. TEETH-GUIDED COMPLIANT JOINT BASED ON CROSS-FOUR-BAR LINKAGE

A. Design of Contact-Aided Finger Joint

Revolute joint is always a common selection, because it is simple to analysis and easy to build. To replicate the polycentric motion of the finger joint that occurs during passive flexion and extension, cross-four-bar linkage is utilized. The above section investigated a key issue of centroides for contact-aided finger joint which would be a good way to mimic human joints. As shown in Fig. 8, the interphalangeal joint of thumb finger has a moving angle ranging from -15 degrees (hyper extension) to 80 degrees (flexion). The hyper extension of -15 degrees are due to safety consideration and passively works. The joint between two finger phalanges is replaced by a cross-four-bar linkage. According to kinematics analysis in Sec. III, the fixed and moving centroides can be determined as shown in Fig. 8. Dotted line sketch shows hyper extension position where the fixed and moving centroides start and intersect. The real line sketch shows the upright finger position which is the rest position of a finger. The final bending position has an angle of 80 degrees that ends the centroides' curves and maximum movement range of the distal finger.

A detailed design of contact-aided cross-four-bar linkage for interphalangeal joint of the thumb finger is shown in Fig. 9. The contact surfaces based on fixed and moving centroides enhance the functionality of the mechanism to be capable of performing certain kinematic tasks as a rigid body. A contact-aided cross-four-bar mechanism is also much higher rigid due to the high kinematic pair between

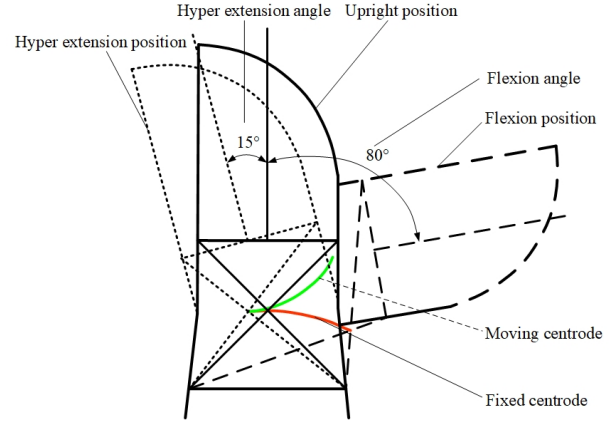


Fig. 8. Interphalangeal joint of thumb finger and its moving and fixed centroides

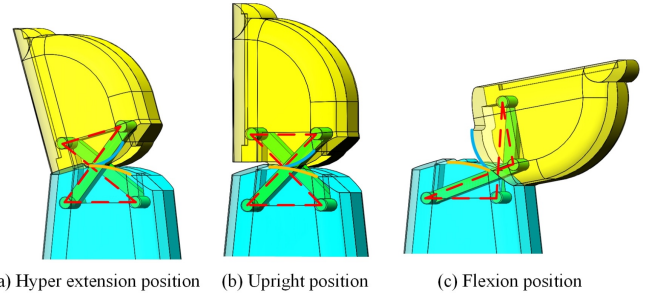


Fig. 9. Interphalangeal joint design of thumb finger with contact-aided cross-four-bar mechanism

two finger phalanges. However, a traditional cross-four-bar linkage comprises four revolute joints and four links. Therefore, designed finger needs very precise manufacturing and external spring for return motion. A method to develop a fully compliant cross links and teeth-guided finger will be presented in next section.

B. Teeth-Guided Compliant Joints

There are many obvious advantages for compliant mechanisms comparing with rigid ones. The smaller number of pin joints can reduce wear or need for lubrication, reduce backlash and increase precision, reduce weight, manufacturing and complexity of assembly. Therefore, compliant mechanisms are considered for many specific applications, such as harsh environment, aerospace, microelectromechanical (MEMS) systems, etc. The construction of compliant mechanism considers either the whole mechanism or some links as compliant/flexible or by replacing only pin joints by flexible hinges while links are kept rigid. Most of flexible finger focus on replacing pin joints with flexible ones, such as Hizook humanoid torso with anthropomorphic hands manufactured by Meka Robotics [36] and Yale open hands[37]. The contact-aided compliant joints utilize distributed compliance approach by replacing crossed rigid links with flexible links. This approach aims to develop a monolithic structure without assembly. The detailed design of one finger joint with distributed compliance is show in Fig. 10. The side two

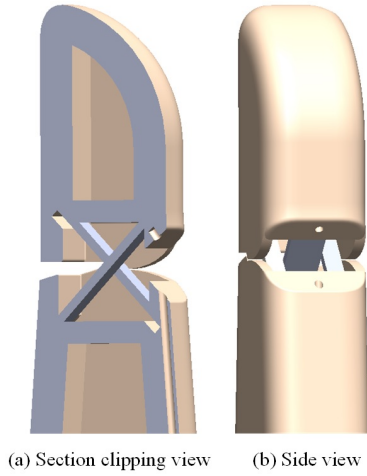


Fig. 10. Detail design of distributed compliant finger joint

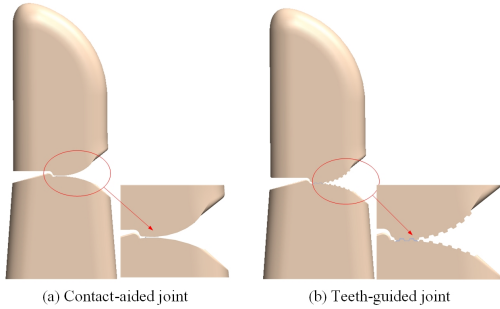


Fig. 11. Contact-aided and teeth-guided compliant joints

pieces of compliant links are identical. Width of centre piece is the same as the sum of side pieces.

For contact-aided cross-four-bar mechanism, contact surfaces based on two centred rolls against each other frictionlessly. However, the motion between two contact surfaces of compliant solution is not the same as rigid design of pure rotation. The sliding between two contact surfaces will influence the precision of the motion of finger. Therefore, an equally distributed teeth-guided compliant joint is presented to obtain a predictable and reliable movement of fingertip, as shown in Fig. 11.

The compliant cross-four-bar linkage undergoes a large and nonlinear deflection. Therefore, nonlinear finite element analysis (FEA) was carried for the compliant cross-four-bar linkages in SolidWorks. Polylactic Acid (PLA) ($E = 3.5e + 009N/m^2$) was applied for both designs. The external force is selected with 80N. No penetration is allowed between two finger phalanges. Simulation results for teeth-guided and contact-aided joints are shown in Fig. 12. The stress simulation results show that maximum stress inside contact-aided joint ($1.350e + 008N/m^2$) is 55.08% larger than maximum stress of teeth-guided joint ($8.705e + 007N/m^2$). The maximum displacement of contact-aided joint ($2.963e + 001mm$) is 62.23% larger than maximum displacement for teeth-guided joint ($1.660e + 001mm$). The maximum strain inside contact-aided joint ($3.558e - 002$) is 30.43% larger than

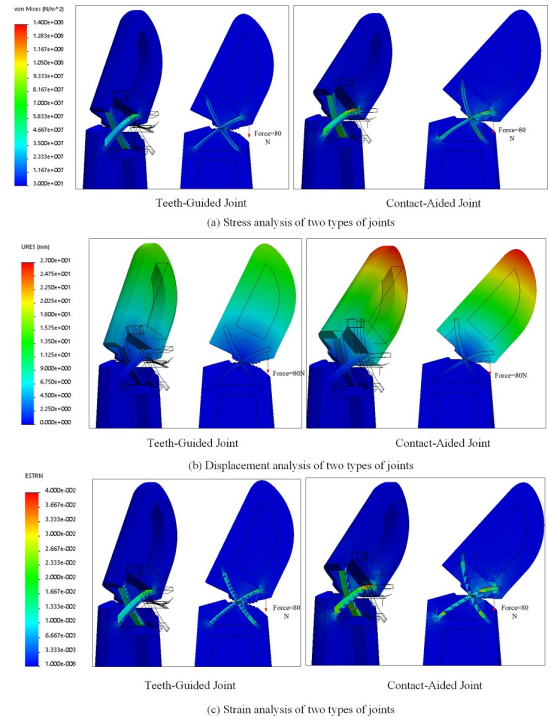


Fig. 12. Finite element analysis of two types of compliant joints

maximum strain of teeth-guided joint ($2.728e - 002$). That means, the teeth on the contact surface distribute partial force applied on the flexible links and work for adjusting the movement of fingertip which make the movement of the fingertip more precise and easier to control.

V. ROBOTIC HAND WITH TWO ANTHROPOMORPHIC FINGERS

Section IV presented development process of a teeth-guided compliant finger joints which distribute driven force and works for precision actuation. This section will focus on developing of a two-fingered hand with anthropomorphic fingers and qualitative discussion. It is obvious that more phalanges can make the object enveloped much easier, an inspired design is shown in [38]. However, according to [39], the output force will decrease from one phalanx to another if the input force is constant. Considering this situation, two phalanges are acceptable for underactuated drive. Figure 13 shows a monolithic finger with two compliant joints. The driven of the finger is carried out by tendon attached on the fingertip.

A. Differential Transmission

The concept of underactuation [40] in robotic gripping with fewer actuators than DOFs allows the two fingers to adjust to irregular shapes without the need for complex control strategies and sensors. Differential mechanisms are used in robotic hands to provide underactuation, such as a movable pulley, seesaw mechanism, fluidic T-pipe and planetary and bevel gear differentials [41]. This differential system always locates at the transforming box of the hand. The most often

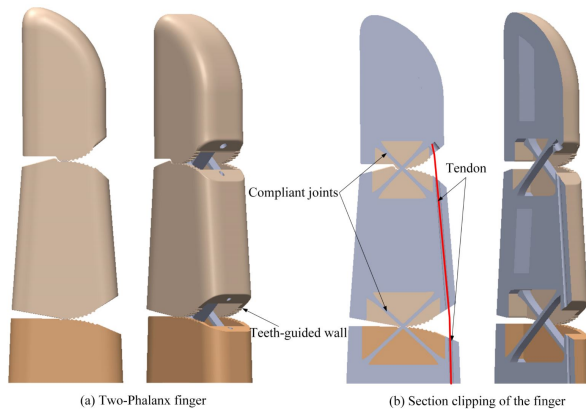


Fig. 13. Anthropomorphic finger with teeth-guided compliant joints

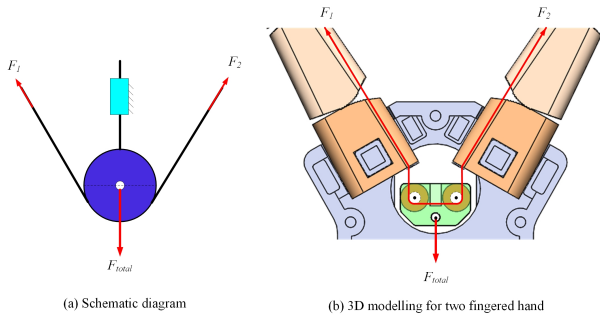


Fig. 14. Differential transmission of two fingered hand

used differential system would be a movable pulley. As shown in Fig. 14, the two ends of the tendon are fixed symmetrically in the two fingers pulley wheels. The actuated power is distributed to the two fingers to facilitate gripping of non-centred or irregularly shaped objects.

B. Robotic Hand with Two Anthropomorphic Fingers

3D modelling of the anthropomorphic hand is shown in Fig. 16. The hand is available for objects grasping with a maximum of 80mm in diameter. The differential mechanism in the hand drive the anthropomorphic finger for grasping of non-centred and irregular objects.

The monolithic finger is shown in Fig. 15. Teeth on the contact surface are also pointed out in Fig. 15(b). The design is available for common desktop 3D printer (Fig. 15(c)). The whole finger is 3D printed in one step with Polylactic Acid (PLA). Most components of the gripper are 3D printed using PLA except digital servo, bearings and metal shafts. There is no need to assemble except fixing tendon on distal phalange of the finger. The weight of the whole anthropomorphic hand is around 300 grams (including actuator). The monolithic finger hand is an affordable and customisable for individual applications.

C. Testing of Robotic Hand

The two-fingered hand is attached on UR5 robotic arm for pick-and-place demonstration. The objective of the testing is to verify the feasibility of the design approach and

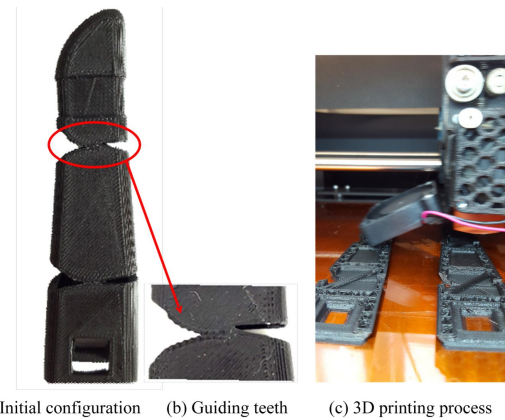


Fig. 15. 3D printed anthropomorphic finger with teeth guided joint

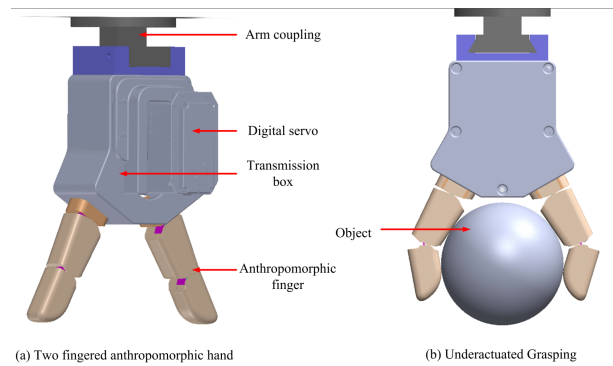


Fig. 16. Two-fingered anthropomorphic hand and underactuated grasping

functionality of monolithic fingers. Silicone tape was pasted on the contact surface to increase friction coefficient between fingertip and objects, but this is a step that is not necessary to create a working hand—indeed ridges can be easily included in the design to improve contact conditions. A series of grasping tasks were conducted to assess the functionality of anthropomorphic fingers. All objects were successfully picked up by the robotic hand as shown in Fig. 17. Some grasping examples are now described.

The main functions of the hand include tip grasping, underactuated grasping, differential grasping due to the inherent characteristics of the hand. The gripping configurations of the hand are determined also by the gripping position and shapes of gripped objects. Such as for large object grasping with a size reaching to the maximum range. There are two types of configurations including tip grasping and underactuated grasping which depend on the grasping position, as shown in Fig. 18. The grasping position in Fig. 18(a) is high, and tip grasping is active. A lower grasping position will induce underactuated grasping [42], [43] with proximal phalange touching the object firstly and following by distal phalange, as shown in Fig. 18(b).

Tip grasping applied for regular shapes grasping is shown in Fig. 19. Small and flat objects with regular shapes such as a blue tape roll in Fig. 19(a), rectangular box in Fig. 19(b) and orange plastic ball in Fig. 19(c), regular size small peach



Fig. 17. Grasping Testing of the two-fingered robotic hand

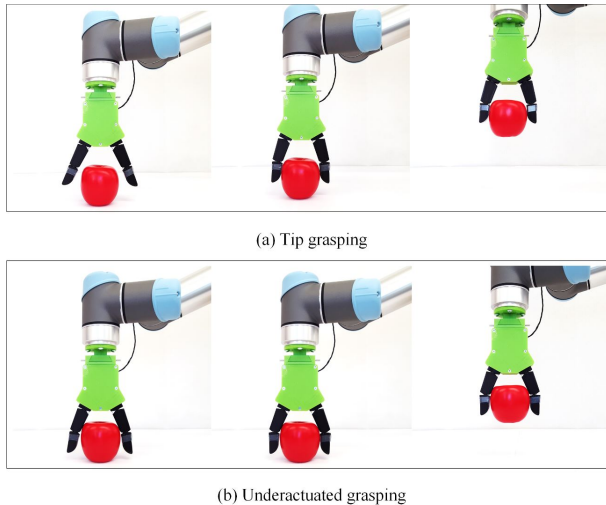


Fig. 18. Grasping configurations depending on locations

in Fig. 19(d).

As shown in Fig. 20, these shapes of objects are irregular that means the mass centre is randomly located. On the other hand, the objects are placed in an asymmetric position. Both result to one finger of the hand touching objects surfaces prior to the other one. Under this situation, differential mechanism will work at initial grasping position. The gripper will return to a proper position after grasping due to compliance of the fingers.

VI. CONCLUSIONS

This paper introduced a monolithic design of anthropomorphic finger based on compliant cross-four-bar joints with teeth-guided contact between phalanges, and the corresponding development process of a two-fingered robotic hand. The teeth-guided solution provides a new way to develop a precisely driven finger. The compliant cross-four-bar conversion of cross-four-bar linkage produces an adaptive finger without assembly. A 3D printed prototype of the introduced concepts was tested by grasping a large range of objects; the results obtained are promising and demonstrate that the monolithic design is feasible. This is a novel approach for developing a category of cost-effective anthropomorphic fingers. Regarding future research work, material selection and reliability need to be considered as well as detailed

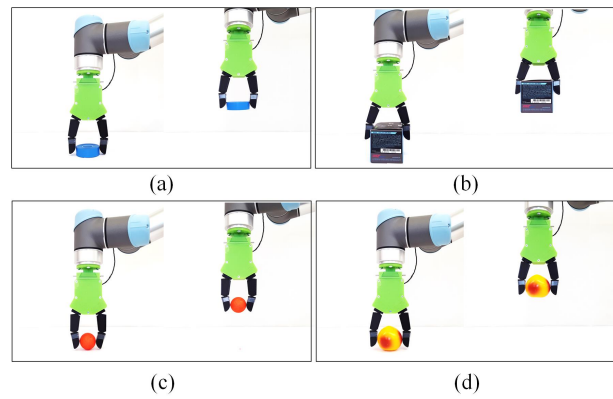


Fig. 19. Tip grasping for regular shapes

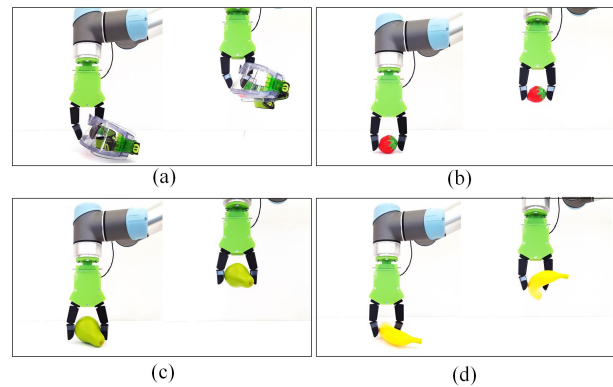


Fig. 20. Grasping for irregular shape objects

characterization of grasping force and grasping performance of robot hands composed of the proposed fingers.

ACKNOWLEDGEMENT

The authors would like to thank Angus Clark, Nicholas Baron and Icey Lu for their help with experimental testing and video editing.

REFERENCES

- [1] J. Napier, *Hands*, Princeton Univ. Press, 1993.
- [2] R. J. Schwarz, C. L. Taylor, The Anatomy and Mechanics of the Human Hand, *Artificial Limbs*, vol. 2, no. 2, pp. 22-35, 1955.
- [3] N. Rojas, A. M. Dollar, Classification and kinematic Equivalents of Contact types for Fingertip-Based Robot Hand Manipulation, *Journal of Mechanisms and Robotics*, no. 8, vol. 4, pp. 041014, 2016.
- [4] Shadow Robot Company. *Shadow Dexterous Hand Now Available for Purchase!* 2015. Available online: <http://www.shadowrobot.com/products/dexterous-hand/> (accessed on 4 June 2015).
- [5] L. U. Odhner, A. M. Dollar, Dexterous Manipulation with Underactuated Elastic Hands, In *Robotics and Automation (ICRA)*, 2011, IEEE International Conference on pp.5254-5260.
- [6] G. Bai, X. Kong, J. M. Ritchie, Kinematic Analysis and Dimensional Synthesis of a Meso-Gripper, *Journal of Mechanisms and Robotics*, no. 9, vol. 3, pp. 031017, 2017.
- [7] R. W. Young, Evolution of the Human Hand: the Role of Throwing and Clubbing, *Journal of Anatomy*, vol. 202, no. 1, pp. 165-174, 2003.
- [8] Z. Xu, V. Kumar, Y. Matsuoka, E. Todorov, Design of an Anthropomorphic Robotic Finger System with Biomimetic Artificial Joints, In *Biomedical Robotics and Biomechanics (BioRob)*, 2012, 4th IEEE RAS EMBS International Conference, pp. 568-574.

- [9] S. Almécija, J. B. Smaers, W. L. Jungers, The Evolution of Human and Ape Hand Proportions, *Nature Communications*, vol. 6, pp. 7717, 2015.
- [10] N. Rojas, A. M. Dollar, Distance-Based Kinematics of the Five-Oblique-Axis Thumb Model with Intersecting Axes at the Metacarpophalangeal Joint, In Rehabilitation Robotics (ICORR), 2017 International Conference on pp. 1331-1336.
- [11] Z. Xu, E. Todorov, B. Dellon, Y. Matsuoka, Design and Analysis of an Artificial Finger Joint for Anthropomorphic Robotic Hands, In Robotics and Automation (ICRA), 2011, IEEE International Conference on pp. 5096-5102.
- [12] Y. M. Moon, Bio-mimetic Design of Finger Mechanism with Contact Aided Compliant Mechanism, *Mechanism and Machine Theory*, vol. 42, no. 5, pp. 600-611, 2007.
- [13] P. A. Halverson, L. L. Howell, S. P. Magleby, Tension-Based Multi-Stable Compliant Rolling-Contact Element, *Mechanism and Machine Theory*, vol. 45, no. 2, pp. 147-156, 2010.
- [14] A. Mottard, T. Laliberté, C. Gosselin, Underactuated Tendon-Driven Robotic/Prosthetic Hands: Design Issues, *Robotics: Science and Systems*, 2017.
- [15] G. Bai, J. Wang, X. Kong, A Two-Fingered Anthropomorphic Robotic Hand With Contact-Aided Cross Four-Bar Mechanisms as Finger Joints, In Conference on Biomimetic and Biohybrid Systems, pp. 28-39, Springer, Cham, 2016.
- [16] Z. M. Li, T. L. Marquardt, P. J. Evans, W. H. Seitz Jr. Biomechanical Role of the Transverse carpal Ligament in Carpal Tunnel Compliance, *Journal of Wrist Surgery*, no. 3, vol. 4, pp. 227. 2014.
- [17] C. J. Shih, C. F. Lin, A Two-Stage Topological Optimum Design for Monolithic Compliant Microgripper Integrated with Flexure Hinges, *Journal of Physics: Conference Series*, vol. 34, no. 1, pp. 840, 2006.
- [18] P. Steutel, G. A. Kragten, and J. L. Herder, Design of an Underactuated Finger with a Monolithic Structure and Largely Distributed Compliance, 2010, ASME International Design Engineering Technical Conferences and Computers and Information in Engineering Conference on pp. 355-363.
- [19] C. H. Liu, C. H. Chiu, Design and Prototype of Monolithic Compliant Grippers for Adaptive Grasping, 2018, 3rd International Conference on Control and Robotics Engineering (ICCRE), pp. 51-55.
- [20] A. Milojević, N. D. Pavlović, N. P. Pavlović, Adaptive Compliant Gripper Finger with Embedded Extending Actuators, *Universitätsbibliothek Ilmenau*, 2014.
- [21] D. Petković, N. D. Pavlović, S. Shamshirband, N. Badrul Anuar, Development of a New Type of Passively Adaptive Compliant Gripper, *Industrial Robot: An International Journal*, vol. 40, no. 6, pp. 610-623, 2013.
- [22] G. Hao, H. Li, A. Nayak, S. Caro, Design of a Compliant Gripper With Multimode Jaws, *Journal of Mechanisms and Robotics*, vol. 10, no. 3, pp. 031005, 2018.
- [23] L. U. Odhner, L. P. Jentoft, Y. Tenzer, Compliant Adaptive Robot Grasper, U.S. Patent 2018/0117773 A1, May 3, 2018.
- [24] M. Muller, A Novel Classification of Planar Four-Bar Linkages and Its Application to the Mechanical Analysis of Animal Systems, *Philosophical Transactions of the Royal Society of London B: Biological Sciences*, vol. 351, no. 1340, pp. 689-72, 1996.
- [25] J. Goodfellow, J. O'Connor. The Knee, W. Norman Scott Mosby-Year Book, Inc, 1994.
- [26] A. Hamon, Y. Aoustin, Cross Four-Bar Linkage for the Knees of a Planar Bipedal Robot, In Humanoid Robots (Humanoids), 2010, 10th IEEE-RAS International Conference on, pp. 379-384.
- [27] Q. T. Truong, B. W. Argyoganendro, H. C. Park, Design and Demonstration of Insect Mimicking Foldable Artificial Wing Using Four-Bar Linkage Systems, *Journal of Bionic Engineering*, vol. 11, no. 3, pp. 449-458, 2014.
- [28] L. Wu, G. Carbone, M. Ceccarelli, Designing an Underactuated Mechanism for a 1 Active DOF Finger Operation, *Mechanism and Machine Theory*, vol. 44, no. 2, pp. 336-348, 2009.
- [29] S. N. Patek, B. N. Nowroozi, J. E. Baio, R. L. Caldwell, A. P. Summers, Linkage Mechanics and Power Amplification of the Mantis Shrimp's Strike, *Journal of Experimental Biology*, vol. 210, no. 20, pp. 3677-3688, 2007.
- [30] J. R. Grubich, M. W. Westneat, Four-Bar Linkage Modelling in Teleost Pharyngeal Jaws: Computer Simulations of Bite Kinetics, *Journal of Anatomy*, vol. 209, no. 1, pp. 79-92, 2006.
- [31] H. D. Eckhardt, Kinematic Design of Machines and Mechanisms, McGraw-Hill, New York, 1998.
- [32] G. Toussaint, Simple Proofs of a Geometric Property of Four-Bar Linkages, *The American Mathematical Monthly*, vol. 110, no. 6, pp. 482, 2003.
- [33] R. L. Norton, Design of Machinery, 5th ed., McGraw-Hill, New York, 2012.
- [34] T. R. Chase, J. A. Mirth, Circuits and Branches of Single-Degree-of-Freedom Planar Linkages, *Journal of Mechanical Design*, vol. 115, no. 2, pp. 223-230, 1993.
- [35] R. S. Hartenberg, J. Denavit, Kinematic Synthesis of Linkages, McGraw-Hill, New York, 1964.
- [36] Meka Robotics. Humanoid Torso and Anthropomorphic Hands, Meka Robotics A2 Compliant Manipulator. <http://www.hizook.com/>
- [37] R. R. Ma, L. U. Odhner, A. M. Dollar, A Modular, Open-Source 3d Printed Underactuated Hand, In Robotics and Automation (ICRA), 2013, IEEE International Conference on, pp. 2737-2743.
- [38] S. Hirose and Y. Umetani. The Development of Soft Gripper for the Versatile Robot Hand, *Mechanism and Machine Theory*, vol. 13, no. 3, pp. 351-359, 1978.
- [39] L. Birglen and C. Gosselin, Kinetostatic Analysis of Underactuated Fingers, IEEE Transactions on Robotics and Automation, vol. 20, no. 2, pp. 211-221, 2004.
- [40] T. Laliberté, C. M. Gosselin, Simulation and Design of Underactuated Mechanical Hands, *Mechanism and Machine Theory*, vol. 33, no. 1-2, pp. 39-57, 1998.
- [41] L. Birglen, C. M. Gosselin, Force Analysis of Connected Differential Mechanisms: Application to Grasping, *The International Journal of Robotics Research*, vol. 25, no. 10, pp. 1033-1046, 2006.
- [42] N. Rojas, R. R. Ma, A. M. Dollar, The GR2 Gripper: an Underactuated Hand for Open-Loop In-Hand Planar Manipulation, IEEE Transact. Robotics, vol. 32, no. 3, pp. 763-770, 2016.
- [43] L. Birglen, T. Laliberté and C. M. Gosselin, Underactuated Robotic Hands, Springer, 2007.